Nano World Journal

https://doi.org/10.17756/nwj.2022-s1-024

Research Article

Open Access

Recent Advances in the Computational Techniques to Predict Structural Properties of ZnS Nanoparticles

Vishakha Sharma[1], Priyanka Kumari[1], Saikat Chattopadhyay[2], and Susruta Samanta[1*]

[1]*Department of Chemistry, Manipal University Jaipur, Rajasthan, India*

[2]*Department of Physics, Manipal University Jaipur, Rajasthan, India*

***Correspondence to:**
Susruta Samanta
Department of Chemistry, Manipal University Jaipur, Rajasthan, India
E-mail: susruta.samanta@jaipur.manipal.edu

Received: August 23, 2022
Accepted: November 02, 2022
Published: November 04, 2022

Citation: Sharma V, Kumari P, Chattopadhyay S, Samanta S. 2022. Recent Advances in the Computational Techniques to Predict Structural Properties of ZnS Nanoparticles. *NanoWorld J* 8(S1): S137-S146.

Published by United Scientific Group

Abstract

In recent decades, nanoparticles have attracted a lot of interest among researchers in various fields. They can influence an atom's atomic, electrical, and magnetic characteristics. Alongside traditional characterization techniques, several computational approaches were developed starting from the 1990s to forecast their atomistic characteristics on a scale that might be challenging to predict from experimental methods. One of these is the Molecular Dynamics (MD) simulation approach, which is used to estimate the atom's structural dynamics during coarsening and aggregation. In this paper, we provide a detailed overview of the zinc sulphide (ZnS) nanoparticles and their structural characteristics as determined by MD Simulations. ZnS is a semiconductor with two polymorphs, Sphalerite and Wurtzite, which may be interconverted under appropriate circumstances. We assess the applicability of computer simulations to predict the mechanical characteristics of ZnS using a variety of interatomic potentials. We also discuss the use of parallel processing and several examples of new advancements in MD simulation techniques. We discuss several processes such as nanoparticle aggregation, nanoparticle coarsening, and phase change to name a few. We also compare experimental data with the simulation model to emphasize the applicability of computational techniques in nanoparticle and semiconductor research.

Keywords

Computational techniques, Molecular dynamics

Introduction

ZnS belongs to the II-VI semiconductor family [1, 2], and possess a large band gap [3, 4]. Zinc (Zn) and Sulphur (S) are present in a *tetrahedral* geometry in ZnS [5-7]. The semiconductor and their alloy in Wurtzite or Zincblende (also known as Sphalerite) are used in electro-optical and electro-acoustic devices [8, 9]. Zincblende are referred to as cubic phase of prototype of II-VI semiconductor like ZnS, ZnSe, and ZnTe which occur as minerals [8]. ZnS form a major component for extraction of Zn [10]. Zn and S play a crucial role in many biological systems by transporting these two materials within the earth and the biological systems [11]. ZnS is used as a part of thin film electroluminescence devices, solar cells [12], photochemical production of hydrogen, IR windows [13, 14], photo catalysts [15], sensors and LASERs, quantum devices[16], environmental sensors[17], and protective coating[18]. The nanoparticles of ZnS are stable at the room temperature for a long period of time – even after 9 months there is no noticeable change in the diffraction pattern [6]. Beside ZnS nanostructures, various other structures are also reported like nanowires, nanobelts, nanocables, and nanosaws [15, 16].

ZnS is comprised of two polymorphs – Sphalerite and Wurtzite [5, 19, 20]. Sphalerite polymorphs are stable and have cubic structure [5, 19, 20]. These have three-layer repeat (*xyz*) along the (111) axis [21]. Wurtzite shows hexagonal structure [5,19, 20] and have two-layer repeat (*xy*) along the *z* axis [21-23]. The relative stability of both the structures changes with the band gap depending on the particle size [5]. Wurtzite nanoparticles, which are smaller than 7 nm, are more stable when compared to Sphalerite nanoparticle in vacuum at 300 K [24-27]. This can be stabilized by adsorption of water on the surface of ZnS nanoparticles [26]. ZnS binds with water to form Zn–O bonds. ZnS nanoparticles adsorb more water molecules in comparison to bulk ZnS. The results from the MD simulations help in determining that the water binding energy is inversely proportional to the surface coverage by water. The order of the strength of the interaction of water follows the trend: isolated nanoparticles > aggregated nanoparticles > bulk crystals. Temperature Programmed Desorption is a method used to calculate the bonding strength between ZnS nanoparticles and water molecules. It states that ZnS nanoparticles are produced by hydrothermal coarsening of bulk ZnS at 250 °C for 3 days [28]. Vogel synthesized ZnS nanoparticles and stabilized them by using mercaptoethanol and the product was a mixture of 2 - 3 nm Sphalerite-Wurtzite type nanoparticles in equal proportion. Thioglycerol stabilizes 2-3 nm ZnS nanoparticles which exist in Sphalerite phase [10]. ZnS particles of size 3 nm have highly distorted structure [24]. To convert the disordered surface to an ordered form, it is solvated with water. This is a reversible process i.e., by solvating with methanol the surface can be disordered again [26].

ZnS is formed biologically in anaerobic environment where sulphide is sourced by sulphate reducing bacteria and the accumulated ZnS forms a saturated solution and eventually precipitation occurs. The natural solution contains tetrameric $Zn_4S_6(H_2O)_4$ in cluster form which have similar structure to Sphalerite [7]. Landing and Lewis found that neutral and anionic species of ZnS are also found in sulfidic water of the Black Sea in which the concentration of sulphide is more as compared to Zn and therefore, the anionic complexes dominate [29].

ZnS clusters are also found in open bubble structure with atoms having three coordination sites [19]. A hollow interior is covered by 4-, 6-, and 8-atom rings creating a shell arrangement with varied bond angles and bond distances [19, 20, 30]. The Euler's law can be utilized to determine the number of rings:

$$N_{6-ring} = n - 4 - 2N_{8-ring} \quad N_{4-ring} = 6 + N_{8-ring} \dots\dots\dots (1)$$

The equation shows that the number of vertices added with number of faces will result in the number of edges plus two [19, 20]. $(ZnS)_{60}$ and $(ZnS)_{50}$ both have onion like structure whereas $(ZnS)_{70}$ and $(ZnS)_{80}$ have double-bubble like structure. The bubble-like structures are stable for n = 10 - 80. To distinguish between the bubble-like structure and the bulk, vibrational spectra can be used which shows a characteristic peak at 320 cm^{-1} for 4 coordinated atoms [19]. Use of Global Minimization Technique proves that bubble clusters are more stable as compared to bulk e.g., stoichiometric clusters [20].

On increase of sulphide concentration, $Zn_2S_3^{2-}$ is formed (Figure 1a). The geometry of this molecule was calculated by the program HYPERCHEM[31]. In this structure the trigonal plane is composed of sulphide ions, but they do not bind to each other instead the sulphide ion forms a bridge between the Zn(II) atoms which in turn bind with the water molecule to satisfy the four-coordination number for Sphalerite and Wurtzite. The terminal ligand can be water, chloride ion, or hydroxide ion. The model calculation shows that the bond length of Zn–S is 2.303 Å. The geometry of $Zn_2S_3^{2-}$ cannot serve as a structural alternative for Sphalerite and Wurtzite as these minerals are formed of six membered rings (Zn_3S_3) (Figure 1b) and not of four membered rings (Zn_2S_2). Like Sphalerite, a structure was proposed for $Zn_4S_6(H_2O)^{4-}$ (Figure 1c), which has a bond distance of 2.254 Å. It is shorter than Zn_3S_3 (2.303Å). The bond distance of Sphalerite and Wurtzite is 2.34 Å which means the soluble complex is smaller when compared to the bulk. The structure shows bond angle of 109.8° for Zn–S–Zn and 109.1° for S–Zn–S. These angles are very close to the bond angle (109.5°) in Sphalerite and Wurtzite [7].

Crystals of both ZnS and Cadmium sulphide (CdS) exist in two forms i.e., Wurtzite and Sphalerite/Zincblende structure which differ from each other mainly at the relative position of the third neighbor. Optical, electronic, and mechanical

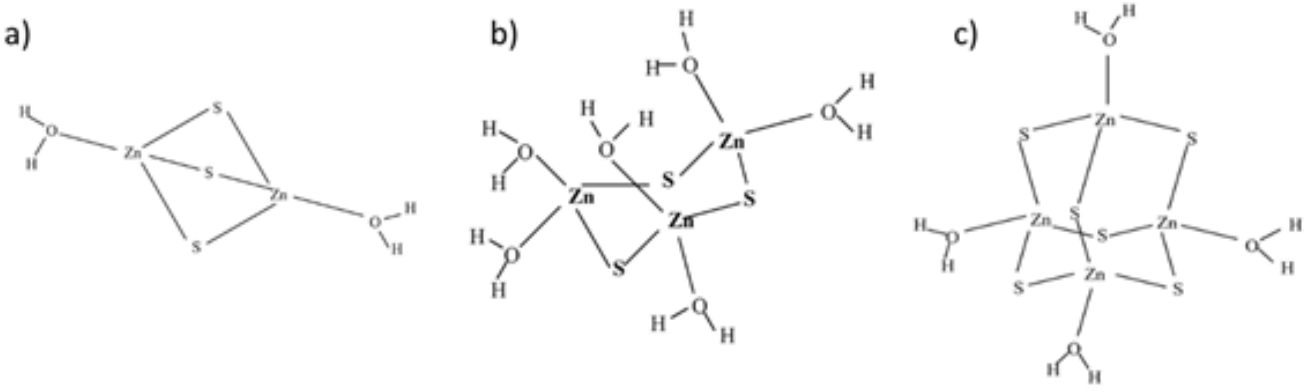

Figure 1: (a) Structure of $[Zn_2S_3(H_2O)_2]^{2-}$, (b) Stable structure of $[Zn_3S_3(H_2O)_6]^0$, (c) Structure of the cluster $[Zn_4S_6(H_2O)_4]^{4-}$.

properties of Zincblende are less studied under high pressure and temperature than Wurtzite as Zincblende is generally more amenable to doping because of its cubic structure. To understand the nature of Zincblende under high temperature, various microscopic modelling and simulation are used. One of the technique involved in this process is MD simulation [8].

Molecular Dynamics Simulation and its Characteristics

In the '90s, simulation of oxides and silicates had been done, but there was no experimental study on sulphide minerals to benchmark the computational findings. Initially, many difficulties arose to establish the interaction between S and many cations because of the fact that bonding in these minerals are of ionic in nature. Computational techniques were successful in studying the defects. These techniques firstly used CASCADE to calculate defect in both polymorphs (Sphalerite and Wurtzite) [32]. Studies showed that the most favorable defect in ZnS is the Schottky defect and least favorable defect is the Frenkel defect [21]. Computational studies of ZnS were generally focused on the effect produced due to the presence of activators on the surface properties. The influence of lead, iron, and copper on surface properties was studied using quantum mechanical method [3]. Computational approach provides a clear electronic and atomic picture of the materials and can clearly predict their influence on structure, synthesis, properties, and performance [8, 9, 33]. Computational techniques involve methods like Electronic Structural Calculations, Kinetic Monte Carlo method, Molecular Orbital calculations, Density Functional Theory, and MD method. All of these are part of multiscale simulations [34].

MD simulation is a widely used computational technique to study the motion of atoms that further makes it easier to understand the structural, dynamic, kinetic, and equilibrium properties under specific conditions [24, 35, 36]. It is a direct simulation technique at the atomic level of the materials [8, 18, 24, 37]. MD simulation is used to study the motion and structural changes in nanoparticles in the process of aggregation and coarsening. The interaction forces help these nanoparticles to undergo translational and rotational movements that aids in finding better suitable location for the aggregation [24]. It is suggested that nanoparticles will adopt a structure that will minimize its energy [1]. Previously, atomic simulation methods were used to calculate the total energy of any system in terms of atomic coordinates [21, 38]. Lippens and Lannoo were the first one to report the theoretical studies on ZnS nanoparticles by employing tight binding approximation for the calculation of band gap of ZnS crystals [1, 39]. Behrman et al. were among the first researchers to carry out studies on II-VI semiconductor compound clusters [40]. They suspected that the data collected from MD simulations were obtained by the use of empirical pseudopotential that was fitted to the macroscopic data, and hence, it might not be accurate to use. They performed both MD simulation and Molecular Orbital calculations on the crystals [1, 40]. Zhu and Averback used MD simulation to sinter copper nanoparticles and found that misaligned nanoparticle rotates to form low energy interface during sintering [41]. Latapie and Farkas use MD simulation to crack tip the starting point for stress induced phase transformation in nanocrystalline iron [42]. Wilson et al. studied pressure induced phase transformation in model bulk metal halides [24]. Anwar and Boateng used MD techniques to simulate the nucleation of Model System [43]. Hamad et al. and Feigel et. al. reviewed some of the computational studies on ZnS nano structures with the help of MD simulation [3].

The atomistic simulation method proved itself in solving various problems, but its applicability is restricted by two factors, i.e., accuracy in modelling interatomic interaction and computational demand. Quantum mechanics states that energy related problems can be solved by solving the Schrödinger wave equation, but this approach is feasible only for simple and small systems. For system beyond hundreds of atoms, it is impractical to use the quantum mechanical method because of the computational expense of first principal method that serves as a limitation. So, the best alternative remain for this process is Molecular Mechanics method that use empirical potential and laws of classical mechanics to predict atomic structure, their interactions, and also produce accurate results [3]. Simulation of complex systems can be done with the help of MD simulation with limited computational demands [44]. This method proved to be promising for the study of atomic level evolution of large systems in a standard time periods (nanoseconds) and provide realistic dimensions [3]. MD simulation can be used to predict almost all the physical properties of materials [8,9,18]. Various thermodynamic data can be determined with the help of MD simulation viz., average configuration energy, temperature, pressure, radial distribution function, and structural factors [3,44]. It has a wide application in solution chemistry as well [43]. It can even function at high temperature, pressure, and for systems of nanometric scale [24]. In the last two decades research showed that MD simulation proved to be an important tool to investigate non harmonic effects in solids [8]. MD simulations are used for simulation of complex systems having a large number of atoms [8,9,33]. It is done to determine the Tersoff Potential for solid structure under the influence of temperature and pressure [8, 9, 18, 33]. MD simulations are effectively used to predict the effect of inter-particle contact after aggregation [45]. Other work done beside these on ZnS nanostructure involved equilibrium configuration of nanoparticles and nanowires, pressure, and temperature effect on structural transformation of nanoparticles, and mechanical properties of ZnS Nanowires [3].

MD simulation method showed many developments specially in parallel platform and computational algorithm like Smoothed Particle Mesh Ewald and Domain Decomposition parallelization for long range force system [46]. Due to its increasing development in new algorithms MD has now entered in other scientific areas viz., electronic structure in the solid state physics [44]. This simulation functions based on interaction potential between the atoms [9,18] and its level of accuracy depend on the empirical potential which is used to predict interatomic interactions. Many empirical potentials are proposed for ZnS. To choose an appropriate empirical potential, researchers have compared their ability to reproduce certain properties for ZnS and used it as a criterion of selection [3].

Various interatomic potentials are used to calculate the structural and mechanical properties of ZnS and then the resultant values are compared to the experimental ones. It is easy to predict material properties using a powerful force field. Major potential functions used were Lattice Static Simulation [5], Atomistic Simulation [3], Interatomic Potential [47], Pair Potential [48], and Tersoff Potential [8].

Lattice Statics simulation is used for minimization of the total energy of the lattice to evaluate surface structure and employing interatomic potential [5]. It helped in studying the surface structure of ZnS and other nanoparticles. It serves as a good option for potential derivation procedure and are optimized by fitting to experimental values which are generally derived at room temperature [3]. Interatomic Potential is used to define the long-range attractive and short-range repulsive forces existing between the atoms in solids [47] and to check the mechanism of uptake of impurities (e.g., cadmium, francium, manganese, etc.) in Sphalerite [3]. Pair Potential was mainly developed for CdS and ZnS crystals. These can be used to measure the lattice and elastic constant for bulk CdS and ZnS in Wurtzite and Rocksalt crystal structure [48] and to study pressure induced phase transformation [3]. Atomistic simulation is the main approach for calculation of the elastic constant and generally, it is done by two methods:

The first method is based on strain fluctuation which functions on the principle that the elastic constant is the second derivative of the deformation energy.

$$\sigma_{ij} = \frac{\partial U}{\partial \epsilon_{ij}} \rightarrow C_{ij} = \frac{\partial^2 U}{\partial \epsilon_i \, \partial \epsilon_j} \ldots\ldots\ldots (2)$$

where, U is the deformation energy, ϵ is the strain, σ is stress, and C_{ij} is the corresponding elastic constant

The second method or the direct method is used to calculate the elastic constant by stress-strain relation of materials. It is based on the principle of constant pressure MD simulation. However, in MD simulation, we need to use average values to determine the stress-strain behavior. Several studies have been done where scientists used the GULP code and applied it on fluctuation method in lattice dynamic calculation [49, 50]. Pressure MD Simulation have been used to calculate the lattice constant value at 300 K and 0 GPa within DL_POLY classic code [51]. From these simulations, primarily three crystal structures of ZnS were reported i.e., Zincblende, Wurtzite, and Rock salt structures. With all the collected experimental data, the conclusion was drawn that lattice static simulation has better results for experimental lattice constant and different mechanical properties of these ZnS phases [3].

The Tersoff Potential (Three Body Potential) is based on the bond ordering principle. The potential does not go far than the atomic distance of the first neighbor. Therefore, it has a very short-range nature. Zn atom has four neighbors viz., S, Zn, S, Zn at distances $\sqrt{3}a/4$, $\sqrt{2}a/2$, $\sqrt{10}a/4$ and a, while the four neighbors in case of ZnS blende are at a distance of 2.343 Å, 3.825Å 4.277Å, and 5.41 Å. The atomic distance in Wurtzite and Zincblende are similar due to their similar densities. Rock salt ZnS comprises of a more compact phase, and therefore shows a noticeable high three-body cutoff. These properties of Rock salt can be improved by changing the three-body cutoff but in case of Wurtzite the changing three-body cutoff has no significant effect other than on C_{11} and C_{33} [3].

Different models e.g., the Shell Model is used in Lattice Simulation, Atomistic Simulation, and Interatomic Potential to add the prioritization effects. In this the ions are assumed to have 2 parts: a) the core (atomic mass), b) shell (polarizable charge). The sum of the core and the shell provides the total charge of the ion.

$$V_{core-shell} = \frac{1}{2} k_s r^2 \ldots\ldots\ldots (3)$$

The use of the Shell Model in MD simulation can be disadvantageous in many ways as it makes MD simulation more complicated by introducing new species into the system and thus, led to increase in the simulation time. Besides, the shells handling need lots of care especially at higher temperature and pressure. Studies were done to visualize the effect of removing the Shell Model and Four Body Potential on the material properties. Results show that removing the Four Body Potential will not create a significant difference in structural and mechanical properties, but removal of Shell Model does show specific effects on Zincblende and Wurtzite properties [3]. The Ewald Summation Method is used to calculate the long-range Coulombic Interactions [52].

Parallel Processing

Among the other development of MD, parallel processing technique is one of the most recent advancements. Parallel processing involves various unique concepts:

i) Load balancing indicates the use of each node simultaneously to an equal degree while executing program on a parallel computer otherwise it can lead to a major wastage of computational resources.

ii) Communication denotes the passing of data while running a program. For better results the communication amount should be the minimum. It is a representation of non-productive operation. The efficiency of the algorithm is directly influenced by the amount of communication.

iii) Scaling has a direct connection to computational performance i.e., speed of processing. If number of nodes increase on the parallel computer, it lead to improvement in performance [44].

Two major algorithms are used in MD simulation. The first one is Replicated Data Algorithm and it is commensurate with effective range of empirical pair potential. According to specific computers, the empirical parameter describing the performance of algorithm changes. Here, $T_s = T_p + T_c$, where time required for each MD time step is total of time of performance of calculation and communication time. It is required to minimize both T_p and T_c to design parallel MD. The above equation can be written as,

$$T_s = T_p(1 + R_{cp}) \ldots\ldots\ldots (4)$$

therefore, $R_{cp} = T_c/T_p$. The ratio of T_c and T_p stand as a very useful measure to calculate efficiency of the algorithm. The efficiency of the parallel programs decreases if numerical processing increases therefore R_{cp} should generally be as small as possible [44].

The second algorithm is Systolic Loop Algorithm and it is suitable for simulations having range of forces in commensuration with sample size of system. This states that if number of atoms are fixed and if the number of nodes is increased, the algorithm decreases in efficiency [44].

The third algorithm is the Parallel Link-Cell Algorithm and it is suitable for systems having a shorter effective range of force between constituent atoms than the sample size. The rate at which Parallel Link-Cell algorithm reached the maximum efficiency is comparatively slower than Replicated Data and Systolic Loop Algorithm algorithms. here also the efficiency is dependent on number of nodes [44].

The DL_POLY Code

It is a parallel MD Simulation package which constitute of highly efficient method and algorithm like Linked Cell, Trotter derived Velocity Verlet [53]. It is a general-purpose MD Simulation software [46, 53], which was developed to simulate system having millions of atoms and is based on the idea of domain decomposition [54]. This programme integrates several modern numerical techniques. The project was started in 1994 with the purpose of utilizing the computers to the fullest advantage and has went through several improvements [46, 53]. Many simulations codes were developed to create a high degree of realism at minimal cost and finally FORTRAN 90 was chosen as a language for the code and to avoid all error proneness of C/C++ [53]. DL_POLY_3 parallelization is an extension of Linked Cell method of Hockney and Eastwood which consist of division of simulation cell into sub cells (Figure 2a), in which the atom can interact with the atom present in same sub cells or with an immediate neighbour. The major communication step in DL_POLY_3 is exchange of Halo Data [46, 53] (Figure 2b). Based on material and ion types, the total number of atoms in an empty box can measure up to one million atoms [54]. DL_POLY_3 contains high level of portability as it compiles only FORTRAN 90 Compiler and complementary Message Passing Interface to handle the communication [53].

Processing and evolution of radiation cascade on nanometer and picosecond scale are assisted by these simulation technique [54]. It involves implementation of Variable Time Step, pseudo and defect detection algorithms.

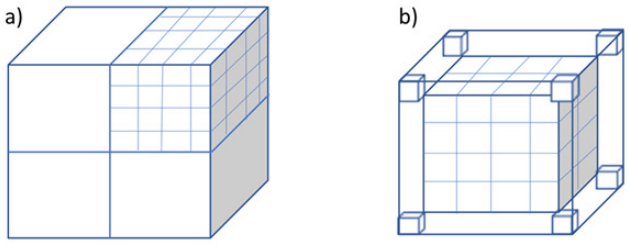

Figure 2: Representation of DL_POLY_3 link cell and domain decomposition. (a) Shows division of simulation cell into domains (larger cubes) and further into link cells (smaller cubes). (b) Shows halo data around domain. Small cubes consist of atomic data of neighboring domain.

Variable Time Step is an option that is majorly used in default values of Maxdix and Mindis which are used as control values in variable time step algorithm. It helps in predicting the greatest distance that a particle can travel in a timestep during simulation [53]. An initial guess by the user for reasonable timestep is required in this option. Pseudo algorithm attaches a Langevin thermostat at the MD cell boundaries [55]. It is necessary to specify the width of thermostat buffer for the user. According to the rule: $2\,\text{Å} \leq d \leq width/4$. The algorithm is applied in two stages, where first stage involves the generation of random forces for all particle in the thermostat buffer and the second stage include the rescaling of kinetic energy of the thermostat bath to make sure that at the end of the simulation, the kinetic energy of the particles shows Gaussian distribution with respect to the temperature targeted. The algorithm works by relaxing the buffer region of system on local scale and dissipating the excess kinetic energy from rest of the system therefore creating a pseudo infinite environment around the MD cell [53]. The defect detection tool is used on algorithm that works by comparing the simulated MD cell to reference MD cell where the first one determines the actual position of particle while the other tells the structure of undamaged lattice.

Molecular Dynamics Simulation of Zinc Sulphide

The idea of the synthesis of ZnS in the aqueous media is important to understand the basis of the simulation. One of the popular methods include mixing of equimolar aqueous solutions of a soluble salt of Zn ($ZnCl_2$ or $ZnSO_4$ is commonly used) and Na_2S (sodium bisulphide) [4]. At specific time gap, the deviation in structure of ZnS is checked to monitor the particle formation. Experimental results show that the structure of the particles after 24 hours of stirring have similar shape and size as that of the particles formed after only 2 hours [56]. Methanol is weaker than water as a polar solvent. Therefore, it is expected that the interaction between ZnS and methanol is comparatively weaker than the interaction of ZnS and water. To check this theory, MD simulation was performed [23]. Before the addition of water (only in the presence of methanol), particles demonstrate typical characterizations, and those results were shown in Table 2. The effects of the addition of water on the ZnS nanoparticles were shown in Table 3.

To get a clear idea about the initial and final structures, MD simulation was performed on particles of different sizes (2, 2.5, 3, 4, and 5 nm) and the variation in the amount of water coverage (1, 3, and 5 water molecules per nm^2 ZnS surface) was also checked [23]. The timestep for the MD simulation was set at 5×10^{-4} ps. In every case, the calculated size of the particles was in close agreement with the actual size of the nanoparticles. The particles of size 2.5 nm and 3 nm show better agreement with the experimental results. The interaction between ZnS particles and water results in the depletion of interfacial energy. To increase the crystallinity in MD simula-

Table 1: Different properties of Wurtzite and Sphalerite polymorphs.

Sr.No.	Properties		Wurtzite	Sphalerite	References
1.	Geometry		Hexagonal	Cubic	[67]
2.	Stability		1300 K	Low Temperature	[68]
3.	Lattice Parameter		3.82 A°	5.32 A°	[69]
4.	Zn-S Distance		2.32/2.42 A°	2.38 A°	
5.	Band gap		3.77 eV	3.72 eV	[67, 68]
6.	XRD	Major Peaks	(100), (101), (102), (110), (112)	(111), (220), (311)	[68]
		Particle size along with temperature	1.5, 3, 6, 9 nm (150, 180, 200, 230 °C)	2, 3, 6, 11, 17 nm (135, 150, 165, 175, 200 °C)	[15]
7.	TEM (Particle size at 200 °C)		~6 nm	~15 – 20 nm	[15]
8.	HRTEM (Particle size)		~6 nm	~3 nm	
9.	PL (excited by 350.7nm laser line)		485 nm	530 nm	[69]
10.	HOMO-LUMO Band gap	Calculated	3.88 eV	3.16 eV	[69]
		Experimental	3.59 eV	3.40 eV	
11.	Ist Ionization Potential Energy (IP$_s$)		6.95 eV	7.15 eV	[69]

Table 2: Characterization of ZnS nanoparticle before adding water (in presence of methanol).

Sr. No.	Techniques	Results	Reference
1	XRD	No structural change (methanol evaporates)	[57]
2	Thermal Desorption Measurement	Showed that methanol is retained by nanoparticle surface and evolved after 50 °C	
3	EXAFS (Extended X-Ray absorption fine Structure)	After 50 °C, particle shows slight deviation in structure as compared to in presence of methanol.	

Table 3: Characterization of ZnS nanoparticle in the presence of water.

Sr. No.	Techniques	Results	Reference
1	XRD	Demonstrate structural change	[57]
2	UV-Vis Absorption	Shows unchanged threshold position	
3	TEM	No size change detected	

tion, low water coverage is required [57].

Nanoparticle Aggregation

Nanoparticle aggregation is directly influenced by the condition of sample preparation [2]. One method used to simulate nanoparticle interactions is by using a closed packed arrangement of 5 nanoparticles. The only limitation of this method is that it allows very limited scope for analysis of the nanoparticles during aggregation. The structural representation is by placing 3 nm Sphalerite nanoparticle at 4 corners of a tetrahedron, and one at the center [24]. Nanoparticle aggregation can influence the growth [58, 59], electronic structure, particle structure [45] of both aggregated clusters and adsorbates within the aggregates [27]. The aggregation process also depends on the equilibrium constant of the surface association. Lower value of equilibrium constant of surface association of retards the process of aggregation. For example, nitrate ions aggregate the system at a faster rate than chloride ions. The charge on the particle also affects the electrolyte concentration. At low pH, particles attain more positive charge, and this results in the stability of the system and high electrolyte concentration which is essential for the aggregation process [60]. The ionic strength also affects the aggregation process. Increased ionic strength of the ZnS nanoparticles in solution enhances aggregation [27].

Atomistic Simulation were performed to predict the structural properties of Wurtzite and Sphalerite form of ZnS. These were based on the use of Interatomic Potential function. This approach is used to determine the total energy of system in the terms of the atomic coordinates. Therefore, by minimizing the lattice energy to remove all strains in crystals, the equilibrium position of the ions can be calculated. Lattice energy depends on the electrostatic forces between atoms and short-range repulsive forces due to overlap. The short-range force can be estimated by Buckingham potential [61] or the intermolecular pair potential, which is expressed as,

$$U_{ij} = \sum_{ij} A_{ij} \exp\left(\frac{-r_{ij}}{\rho_{ij}}\right) - C_{ij} r_{ij}^{-6} \dots\dots\dots (5)$$

To simulate the polarizability of the ions, the Shell Model can be used, and to determine the effect of directionality 3 body terms can be included [21]. The angle bend form of the

3-body interaction is determined by the following equation,

$$u_{ijk} = \frac{1}{2} k_{ijk} (\theta - \theta_{ijk})^2 \dots\dots\dots (6)$$

where, u_{ijk} is the interaction potential, θ is the angle formed by i, j, k atoms, k_{ijk} is the model parameter, and θ_{ijk} is the equilibrium bond angle [24].

Interaction in ZnS is determined by the short-range potential parameters by Least Square fitting procedure. The method includes the fitting of the potential function to the experimental data (Sphalerite phase), and minimization of the difference between calculated and experimental data. For the best results, the Buckingham Interactions were combined with the Shell Model and 3-Body term for the S–Zn–S bond. These potentials when used with Wurtzite phase of ZnS produce similar results, but not as good as for the Sphalerite phase [21].

To get the results of particle aggregation, DL_POLY can be used [51, 53]. MD simulation was performed at 300 K using time step of 0.5 fs. The results show that the equilibrium was not reached after ~1.1 ns. During this time, the system undergoes, structural relaxation (~0 – 10 ps), particle aggregation (~10 – 235 ps), particle coarsening (~235 – 480 ps), and phase transformation (after 480 ps). The snapshots of the system at different simulation times, help in predicting the rearrangement of atoms at the surface to reach the energy minima after ~10 ps. The aggregation occurs simultaneously along with rearrangement and fusion of adjacent pairs of nanoparticles. This led to an activation energy of ~10 kJ/mol for the aggregation of ZnS nanoparticles. Therefore, even a small amount of energy can lead to disaggregation of the nanoparticles [24]. The oriented attachment becomes a crucial growth mechanism which affects the aggregation of particles. It involves self-organization of adjacent particles to share a common crystallographic orientation. This mechanism is applicable only when particles are freely moving [62].

Simulation of nanoparticles that have already undergone structural relaxation shows the details of the translational and rotational motions. The rotational and translational motions are the result of non-zero vector forces which depend on the distribution of the nanoparticles in space. The comparison of unrelaxed and relaxed nanoparticles helps in acknowledging that the energy used in aggregation does not come from surface relaxation, instead, it originates from the potential energy that is released during the interaction of nanoparticles to achieve a lower energy rearrangement [24].

Nanoparticle Coarsening

The step following the aggregation process is coarsening via atomic diffusion. Atomic diffusion plays an important role in both coarsening of nanoparticles and structural transformation [35, 37, 63]. Different mobility is possessed by different atoms depending on the site where they are situated. During the simulation, most atoms move ~2.3 Å. Some atoms move about 3.5 Å which clearly indicates that they are present on the surface. Surface diffusion takes place at a faster rate than bulk diffusion. Atomic diffusion is affected by the presence of

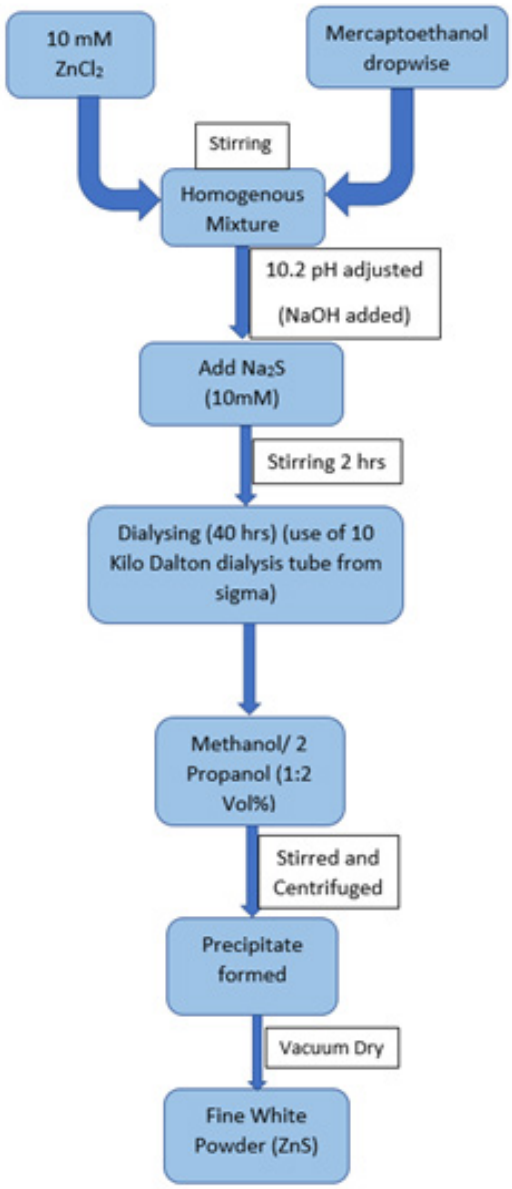

Figure 3: Synthesis of ZnS in aqueous medium.

chemically bound organic molecules or physically absorbed molecules which slows down the coarsening process. The diameter of the particles after coarsening become ~5 nm and a layer is formed on the nanoparticle surface. This results in close packing of the S–Zn–S layers producing Wurtzite (001) structure. The (001) surface Wurtzite has higher surface energy than (100) and (110) Wurtzites. This favours the formation of the Wurtzite (001) over Sphalerite nanoparticles [24].

Ostwald Ripening (OR) is a pathway that refers to the particle growth in solution based on dissolution–precipitation mechanism [27]. The OR crystal growth kinetics can be described by

$$D(t) = D_o + K.t^{\frac{1}{n}} \dots\dots\dots (7)$$

where, D_o is the initial particle size, $D(t)$ is the size of the particle at time t, K is the rate constant for the limiting step, and n is calculated by the nature of the rate limiting step [64].

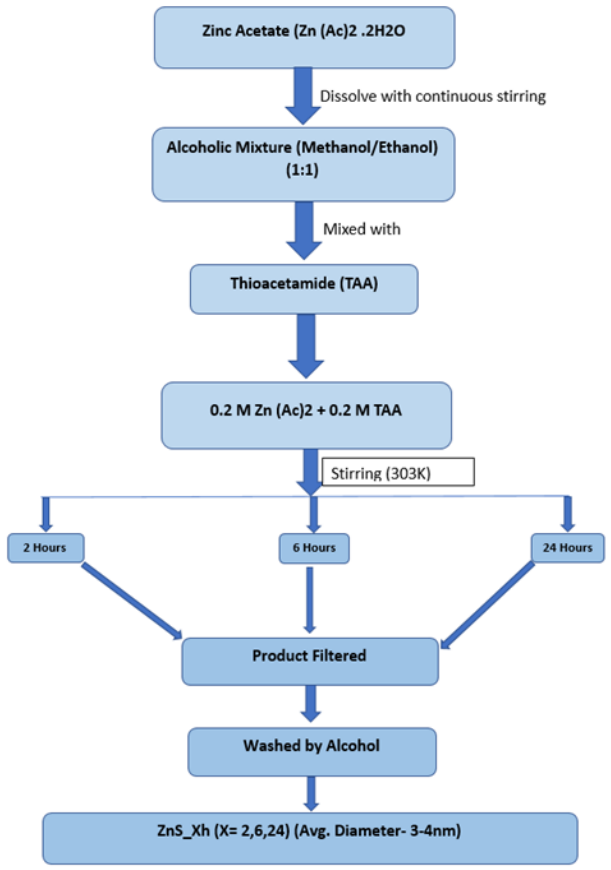

Figure 4: Synthesis of ZnS in methanol medium.

Additionally, because of Oriented Attachment (OA), nanoparticles can orient themselves to attach to each other, and release the associated surface energy. During the coarsening process of uncapped ZnS via hydrothermal technique, OA dominates at the early stages and OR happens throughout the process. In the case of capped nanoparticles (generally done by mercaptoethanol) [6, 27], OA based crystal growth occurs, and OR is suppressed [27]. Due to the low solubility of ZnS, the suspension of uncapped and capped nanoparticles is kinetically stabilized against coarsening at the room temperature. The uncapped nanoparticles which carry surface charge are thermodynamically and kinetically stable against aggregation [27].

Phase Transformation

Phase transformation can occur on the surface, interface, or within bulk based on the particle size, structure, aggregation state, dopant, pressure, and temperature [24, 27, 59]. MD simulation results show that the Sphalerite to Wurtzite phase transformation occurs via surface nucleation. During Wurtzite nucleation, two actions occur simultaneously, i.e., the overlapped Wurtzite (110) and (112) peaks become resolved and characteristic Wurtzite peak (102) and (103) start appearing. Results shows that average bond length of Zn-S (2.33 Å) lies in the close proximity with the bulk Wurtzite (2.34 Å). However, due to the compressive surface stress, most of the Zn-S bonds have bond length of 2.31Å [24]. The bond angles of S–Zn–S are majorly distributed around equilibrium value of Sphalerite and Wurtzite i.e., 109.4° [7]. Few atoms that participate in the bond breakage during the formation of Wurtzite have bond angle close to 90° [24, 27]. The activation energy involved in Sphalerite to Wurtzite transformation is dependent on the reaction area [27]. Thiols, like pentafluoro thiophenol, and 1-decanethiol, 1-hexaenethiol can induce phase transformation in ZnS without changing the crystal size 3 nm. Additionally, acids which have low pKa value can also induce phase transition. Examples include benzoic acid and cyanoacetic acid. Acetic acid or octanoic acid are examples of acids with comparatively higher pKa values and they cannot induce phase transition. In the case of thiols, there is no connection between pKa value and phase transition [65].

Phase Stability

For stability of a phase, minimization of Gibbs free energy is required [27]. The Interfacial free energy can be written as,

$$G(p,T,\gamma) = E - TS + (p+p')V + \gamma A + other\ terms \ldots\ldots\ldots (8)$$

where, T = ambient temperature, p = pressure, p' = excess internal pressure, and A = surface area [66].

Evaluation of γ is important to predict phase stability of small size particles [27]. MD simulation helps in calculating surface energy and surface free energy with the help of which we can predict the average surface free energy value that helps in evaluating the variations in phase stability along with particle size [5, 21, 25, 27]. The surface free energy of a nanoparticle in solution can be deviated by change in ionic strength, pH and surface bound ligands [45]. In the case of ZnS, bulk Sphalerite shows more stability as compared to Wurtzite by $\Delta G_{bulk} \approx 13$ KJ mol^{-1}. Along with this a stability inversion occurs for the particles having size below $D_c \approx 14$ nm. The results of MD also show that the presence of solvent or vacuum can produce deviation in free energy curves due to the presence of water phase. In this case, the stability inversion shifts toward small particle size or completely disappears [27].

Conclusions

In this review, we discussed the importance of computational techniques to reciprocate the findings from experiments. Computational techniques can be very useful to look into the molecular details of the interactions in the nanostructures which can be challenging to characterize experimentally. We looked into the standardization of computational techniques by their efficiency to replicate experimental data and elaborated the usefulness of the techniques to predict physical, structural, and dynamic properties. We also discussed specific popular techniques which are becoming standard methods to predict the properties of nanomaterials. We believe, it will be enlightening to researchers who wish to apply the potential of computational techniques to illustrate minute details of various types of nanostructures.

Conflict of Interest

The authors declare no competing interests.

References

1. Hamad S, Woodley SM, Catlow CRA. 2009. Experimental and computational studies of ZnS nanostructures. *Mol Simul* 35(12-13): 1015-1032. https://doi.org/10.1080/08927020903015346
2. Kumari P, Misra KP, Chattopadhyay S, Samanta S. 2021. A brief review on transition metal ion doped ZnO nanoparticles and its optoelectronic applications. *Mater Today Proc* 43(Pt 5): 3297-3302. https://doi.org/10.1016/j.matpr.2021.02.299
3. Khalkhali M, Liu Q, Zhang H. 2014. A comparison of different empirical potentials in ZnS. *Model Simul Mat Sci Eng* 22(8): 085014. https://doi.org/10.1088/0965-0393/22/8/085014
4. Kumari P, Sharma A, Kumawat A, Samanta S, Misra KP, et al. 2022. Strong UV emission in flakes-like ZnS nanoparticles synthesized by cost effective sol-gel method. *Mater Today Proc* 58: 642-647. https://doi.org/10.1016/j.matpr.2022.01.353
5. Hamad S, Cristol S, Catlow CRA. 2002. Surface structures and crystal morphology of ZnS: computational study. *J Phys Chem B* 106(42): 11002-11008. https://doi.org/10.1021/jp026396d
6. Vogel W, Borse PH, Deshmukh N, Kulkarni SK. 1999. Structure and stability of monodisperse 1.4-nm ZnS particles stabilized by Mercaptoethanol. *Langmuir*16(4): 2032-2037. https://doi.org/10.1021/la9910071
7. Luther GW, Theberge SM, Rickard DT. 1999. Evidence for aqueous clusters as intermediates during zinc sulfide formation. *Geochim Cosmochim Acta* 63(19-20): 3159-3169. https://doi.org/10.1016/S0016-7037(99)00243-4
8. Benkabou F, Aourag H, Certier M. 2000. Atomistic study of zinc-blende CdS, CdSe, ZnS, and ZnSe from molecular dynamics. *Mater Chem Phys* 66(1): 10-16. https://doi.org/10.1016/S0254-0584(00)00239-X
9. Kanoun MB, Merad AE, Aourag H, Cibert J, Merad G. 2003. Molecular-dynamics simulations of structural and thermodynamic properties of ZnTe using a three-body potential. *Solid State Sci* 5(9): 1211-1216. https://doi.org/10.1016/S1293-2558(03)00154-7
10. Zhang H, Banfield JF. 2009. Identification and growth mechanism of ZnS nanoparticles with mixed cubic and hexagonal stacking. *J Phys Chem C* 113(22): 9681-9687. https://doi.org/10.1021/jp902499a
11. Hamad S, Cristol S, Catlow CRA. 2005. Simulation of the embryonic stage of ZnS formation from aqueous solution. *J Am Chem Soc* 127(8): 2580-2590. https://doi.org/10.1021/JA045274R
12. Maity R, Chattopadhyay KK. 2004. Synthesis and optical characterization of ZnS and ZnS:Mn nanocrystalline thin films by chemical route. *Nanotechnology* 15(7): 812. https://doi.org/10.1088/0957-4484/15/7/017
13. Goswami N, Sen P. 2012. UV-Visible spectroscopic study of ZnS nanostructures synthesized by a novel micellar method. J Mater Sci 47(6): 2903-2909. https://doi.org/10.1007/S10853-011-6122-3
14. Calandra P, Goffredi M, Liveri VT. 1999. Study of the growth of ZnS nanoparticles in water/AOT/n-heptane microemulsions by UV-absorption spectroscopy. *Colloids Surf A Physicochem Eng Asp* 160(1): 9-13. https://doi.org/10.1016/S0927-7757(99)00256-3
15. Biswas S, Kar S. 2008. Fabrication of ZnS nanoparticles and nanorods with cubic and hexagonal crystal structures: a simple solvothermal approach. *Nanotechnology* 19(4): 045710. https://doi.org/10.1088/0957-4484/19/04/045710
16. Huang TT, Tan K, Lin MH. 2007. A theoretical exploration of the interaction of adsorptive molecules with the ZnS clusters. *J Mol Struct* 821(1-3): 101-105. https://doi.org/10.1016/j.theochem.2007.06.032
17. Goswami N, Sen P. 2005. Improved crystallinity of zinc sulfide nanoparticles in aqueous environment. *MRS Online Proceedings Library* 879: 8-13. https://doi.org/10.1557/PROC-879-Z3.1
18. Benkabou F, Certier M, Aourag H. 2003. Elastic properties of zinc-blende GaN, AlN and InN from molecular dynamics. Mol Simul 29(3): 201-209. https://doi.org/10.1080/0892702021000049673
19. Hamad S, Richard C, Catlow A, Spanó E, Matxain JM, et al. 2005. Structure and properties of ZnS nanoclusters. *J Phys Chem B* 109(7): 2703-2709. https://doi.org/10.1021/jp0465940
20. Spanó E, Hamad S, Catlow CRA. 2003. Computational evidence of bubble ZnS clusters. *J Phys Chem B* 107(38): 10337-10340. https://doi.org/10.1021/JP035508D
21. Wright K, Jackson RA. 1995. Computer simulation of the structure and defect properties of zinc sulfide. *J Mater Chem* 5(11): 2037-2040. https://doi.org/10.1039/JM9950502037
22. Fleet ME. 1977. Structural transformations in natural ZnS. *Am Mineral* 62(5-6): 540-546.
23. Gilbert B, Zhang H, Huang F, Banfield JF. 2004. Analysis and simulation of the structure of nanoparticles that undergo a surface-driven structural transformation. *J Chem Phys* 120(24): 11785. https://doi.org/10.1063/1.1752890
24. Zhang H, Banfield JF. 2004. Aggregation, coarsening, and phase transformation in ZnS nanoparticles studied by molecular dynamics simulations. *Nano Lett* 4(4): 713-718. https://doi.org/10.1021/NL035238A
25. Zhang H, Huang F, Gilbert B, Banfield JF. 2003. Molecular dynamics simulations, thermodynamic analysis, and experimental study of phase stability of zinc sulfide nanoparticles. *J Phys Chem B* 107(47): 13051-13060. https://doi.org/10.1021/JP036108T
26. Hamad S, Catlow CRA. 2006. Computational study of the relative stabilities of ZnS clusters, for sizes between 1 and 4 nm. *J Cryst Growth* 294(1): 2-8. https://doi.org/10.1016/j.jcrysgro.2006.05.024
27. Gilbert B, Zhang H, Huang F, Finnegan MP, Waychunas GA, et al. 2003. Special phase transformation and crystal growth pathways observed in nanoparticles. *Geochem Trans* 4: 20-27. https://doi.org/10.1039/B309073F
28. Zhang H, Rustad JR, Banfield JF. 2007. Interaction between water molecules and zinc sulfide nanoparticles studied by temperature-programmed desorption and molecular dynamics simulations. *J Phys Chem A* 111(23): 5008-5014. https://doi.org/10.1021/jp0688916
29. Landing WM, Lewis BL. 1991. Thermodynamic modeling of trace metal speciation in the black sea. In: İzdar E, Murray JW (eds) Black sea oceanography. Springer, Dordrecht, pp 125-160. https://doi.org/10.1007/978-94-011-2608-3_8
30. Spanó E, Hamad S, Catlow CRA. 2004. ZnS bubble clusters with onion-like structures. *Chem Commun* 4(7): 864-865. https://doi.org/10.1039/B314104G
31. Froimowitz M. 1993. HyperChem: a software package for computational chemistry and molecular modeling. *Biotechniques*14(6): 1010-1013.
32. Faist J, Capasso F, Sivco DL, Sirtori C, Hutchinson AL, et al. 1994. Quantum cascade laser. *Science* 264(5158): 553-556. https://doi.org/10.1126/SCIENCE.264.5158.553
33. Goumri-Said S, Kanoun MB, Merad AE, Merad G, Aourag H. 2004. Prediction of structural and thermodynamic properties of zinc-blende AlN: Molecular dynamics simulation. *Chem Phys* 302(1-3): 135-141. https://doi.org/10.1016/J.CHEMPHYS.2004.03.030
34. Rustad JR, Dzwinel W, Yuen DA. 2001. Computational approaches to nanomineralogy. *Rev Mineral Geochem* 44(1): 191-216. https://doi.org/10.2138/RMG.2001.44.06
35. Hezaveh S, Samanta S, Milano G, Roccatano D. 2012. Molecular dynamics simulation study of solvent effects on conformation and dynamics of polyethylene oxide and polypropylene oxide chains in water and in common organic solvents. *J Chem Phys* 136(12): 124901. https://doi.org/10.1063/1.3694736
36. Samanta S, Roccatano D. 2013. Interaction of curcumin with PEO-PPO-PEO block copolymers: a molecular dynamics study. *J Phys Chem B* 117(11): 3250-3257. https://doi.org/10.1021/jp309476u
37. Karki KJ, Samanta S, Roccatano D. 2016. Molecular properties of astaxanthin in water/ethanol solutions from computer simulations. *J Phys Chem B* 120(35): 9322-9328. https://doi.org/10.1021/acs.jpcb.6b06055

38. Sayle DC, Mangili BC, Klinowski J, Sayle TXT. 2006. Simulating self-assembly of ZnS nanoparticles into mesoporous materials. *J Am Chem Soc* 128(47): 15283-15291. https://doi.org/10.1021/JA0650697
39. Lippens PE, Lannoo M. 1989. Calculation of the band gap for small CdS and ZnS crystallites. *Phys Rev B Condens Matter* 39(15): 10935-10942. https://doi.org/10.1103/PhysRevB.39.10935
40. Behrman EC, Foehrweiser RK, Myers JR, French BR, Zandler ME. 1994. Possibility of stable spheroid molecules of ZnO. *Phys Rev A* 49(3): R1543-R1543. https://doi.org/10.1103/PhysRevA.49.R1543
41. Zhu H, Averback RS. 1996. Sintering processes of metallic nano-particles: a study by molecular-dynamics simulations. In: German RM, Messing GL, Cornwall RG (eds) Sintering technology. CRC Press, pp 85-92. https://doi.org/10.1201/9781003067566-11
42. Latapie A, Farkas D. 2003. Molecular dynamics simulations of stress-induced phase transformations and grain nucleation at crack tips in Fe. *Model Simul Mat Sci Eng* 11(5): 745. https://doi.org/10.1088/0965-0393/11/5/303
43. Hamad S, Hughes CE, Catlow CRA, Harris KDM. 2008. Clustering of glycine molecules in aqueous solution studied by molecular dynamics simulation. *J Phys Chem B* 112(24): 7280-7288. https://doi.org/10.1021/jp711271z
44. Smith W. 1991. Molecular dynamics on hypercube parallel computers. Comput Phys Commun 62(2-3): 229-248. https://doi.org/10.1016/0010-4655(91)90097-5
45. Huang F, Gilbert B, Zhang H, Banfield JF. 2004. Reversible, surface-controlled structure transformation in nanoparticles induced by an aggregation state. *Phys Rev Lett* 92(15): 155501. https://doi.org/10.1103/PhysRevLett.92.155501
46. Bush IJ, Todorov IT, Smith W. 2006. A DAFT DL_POLY[1] distributed memory adaptation of the Smoothed Particle Mesh Ewald method. *Comput Phys Commun* 175(5): 323-329. https://doi.org/10.1016/j.cpc.2006.05.001
47. Wright K, Gale JD. 2004. Interatomic potentials for the simulation of the zinc-blende and wurtzite forms of ZnS and CdS: bulk structure, properties, and phase stability. *Phys Rev B Condens Matter Mater Phys* 70(3): 035211. https://doi.org/10.1103/PhysRevB.70.035211
48. Grünwald M, Zayak A, Neaton JB, Geissler PL, Rabani E. 2012. Transferable pair potentials for CdS and ZnS crystals. *J Chem Phys* 136(23): 234111. https://doi.org/10.1063/1.4729468
49. Gale JD. 2005. GULP: capabilities and prospects. *Z Kristallogr Cryst Mate* 220(5-6): 552-554. https://doi.org/10.1524/zkri.220.5.552.65070
50. Williford RE, Devanathan R, Weber WJ. 1998. Computer simulation of displacement energies for several ceramic materials. *Nucl Instrum Methods Phys Res B* 141(1-4): 94-98. https://doi.org/10.1016/S0168-583X(98)00066-4
51. Smith W, Yong CW, Rodger PM. 2002. DL_POLY: application to molecular simulation. *Mol Simul* 28(5): 385-471. https://doi.org/10.1080/08927020290018769
52. Darden T, York D, Pedersen L. 1993. Particle Mesh Ewald - an N·Log(N) method for Ewald sums in large systems. *J Chem Phys* 98(12): 10089-10092. https://doi.org/10.1063/1.464397
53. Todorov IT, Smith W, Trachenko K, Dove MT. 2006. DL_POLY_3: new dimensions in molecular dynamics simulations via massive parallelism. *J Mater Chem* 16(20): 1911-1918. https://doi.org/10.1039/b517931a
54. Trachenko K, Dove MT, Artacho E, Todorov IT, Smith W. 2006. Atomistic simulations of resistance to amorphization by radiation damage. *Phys Rev B Condens Matter Mater Phys* 73(17): 174207. https://doi.org/10.1103/PhysRevB.73.174207
55. Dunweg B, Kremer K. 1993. Molecular-dynamics simulation of a polymer-chain in solution. *J Chem Phys* 99(9): 6983-6997. https://doi.org/10.1063/1.465445
56. Berlier G, Meneau F, Sankar G, Catlow CRA, Thomas JM, et al. 2006. Synthesis and characterisation of small ZnS particles. *Res Chem Intermed* 32(7): 683-693. https://doi.org/10.1163/156856706778400334
57. Zhang H, Gilbert B, Huang F, Banfield JF. 2003. Water-driven structure transformation in nanoparticles at room temperature. *Nature* 424(6952): 1025-1029. https://doi.org/10.1038/nature01845
58. Zhang H, Banfield JF. 2002. Kinetics of crystallization and crystal growth of nanocrystalline anatase in nanometer-sized amorphous titania. *Chem Mater* 14(10): 4145-4154. https://doi.org/10.1021/cm020072k
59. Zhang H, Banfield JF. 1999. New kinetic model for the nanocrystalline anatase-to-rutile transformation revealing rate dependence on number of particles. *Am Mineral* 84(4): 528-535. https://doi.org/10.2138/AM-1999-0406
60. Kallay N, Žalac S. 2002. Stability of nanodispersions: a model for kinetics of aggregation of nanoparticles. *J Colloid Interface Sci* 253(1): 70-76. https://doi.org/10.1006/JCIS.2002.8476
61. Buckingham RA. 1938. The classical equation of state of gaseous helium, neon and argon. *Proc R Soc Lond A Math Phys Sci* 168(933): 264-283. https://doi.org/10.1098/rspa.1938.0173
62. Penn RL, Banfield JF. 1998. Imperfect oriented attachment: Dislocation generation in defect-free nanocrystals. *Science* 281(5379): 969-971. https://doi.org/10.1126/SCIENCE.281.5379.969
63. Samanta S, Hezaveh S, Roccatano D. 2013. Theoretical study of binding and permeation of ether-based polymers through interfaces. *J Phys Chem B* 117(47): 14723-14731. https://doi.org/10.1021/jp4028832
64. Borg RJ, Dienes GJ. 1992. The physical chemistry of solids. Academic Press, Boston, USA.
65. Murakoshi K, Hosokawa H, Tanaka N, Saito M, Wada Y, et al. 1998. Phase transition of ZnS nanocrystallites induced by surface modification at ambient temperature and pressure confirmed by electron diffraction. *Chem Commun* 1998: 321-322. https://doi.org/10.1039/A707176K
66. Hill TL. 1962. Thermodynamics of small systems. *J Chem Phys* 36(12): 3182. https://doi.org/10.1063/1.1732447
67. La Porta FA, Ferrer MM, De Santana YVB, Raubach CW, Longo VM, et al. 2013. Synthesis of wurtzite ZnS nanoparticles using the microwave assisted solvothermal method. *J Alloys Compd* 556: 153-159. https://doi.org/10.1016/j.jallcom.2012.12.081
68. Balantseva E, Berlier G, Camino B, Lessio M, Ferrari AM. 2014. Surface properties of ZnS nanoparticles: A combined DFT and experimental study. *J Phys Chem C* 118(41): 23853-23862. https://doi.org/10.1021/jp507963y
69. La Porta FA, Andrés J, Li MS, Sambrano JR, Varela JA, et al. 2014. Zinc blende versus wurtzite ZnS nanoparticles: Control of the phase and optical properties by tetrabutylammonium hydroxide. *Phys Chem Chem Phys* 16(37): 20127-20137. https://doi.org/10.1039/C4CP02611J